Case Studies in Thermal Engineering 49 (2023) 103277

Contents lists available at ScienceDirect

Case Studies in Thermal Engineering

journal homepage: www.elsevier.com/locate/csite

Chemical potential of different phases inside the pyramid stepped basin solar still through Gibbs free energy

S. Shanmugan [a,**], Joy Djuansjah [b], Mahmoud Ahmadein [b,c], Naser A. Alsaleh [b], Seyed Masoud Parsa [d], Ammar H. Elsheikh [c,*]

[a] Research Centre for Solar Energy, Department of Engineering Physics, College of Engineering, Koneru Lakshmaiah Education Foundation, Green Fields, Vaddeswaram, Guntur, 522502, Andhra Pradesh, India
[b] Mechanical Engineering Department, Imam Mohammad Ibn Saud Islamic University, Kingdom of Saudi Arabia
[c] Department of Production Engineering and Mechanical Design, Tanta University, Tanta, 31527, Egypt
[d] Centre for Technology in Water and Wastewater, School of Civil and Environmental Engineering, University of Technology Sydney, NSW, 2007, Australia

GRAPHICAL ABSTRACT

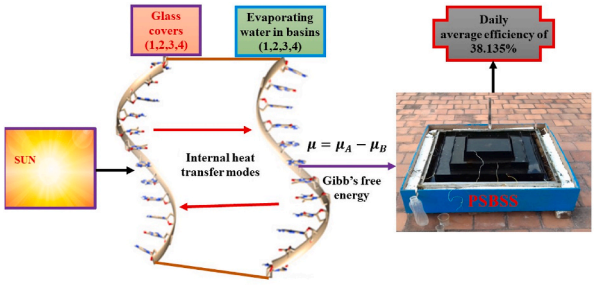

ARTICLE INFO

Handling Editor: Huihe Qiu

Keywords:
Gibbs phase rule
Chemical potential
Solar still
Equilibrium

ABSTRACT

Chemical potentials of the temperature components of the pyramid stepped basin solar distiller (PSBSD) have been evaluated to illustrate the behavior of the water vapor and condensed water droplets during the process of solar distillation. Chemical potential is one of the main criteria in terms of chemical and phase equilibrium which is obtained from the Gibbs phase rule. The application of the Gibbs phase rule established a good relationship between the design, climatic and experimental parameters of the PSBSD. The internal heat transfer coefficients of the distiller are influenced by the intensity of solar radiation and ambient temperature which in turn explains the intensive state of the PSBSD. It is found that the chemical potentials and the intensive states of

* Corresponding author.
** Corresponding author.
E-mail addresses: s.shanmugam1982@gmail.com (S. Shanmugan), ammar_elsheikh@f-eng.tanta.edu.eg (A.H. Elsheikh).

https://doi.org/10.1016/j.csite.2023.103277
Received 14 May 2023; Received in revised form 3 July 2023; Accepted 9 July 2023
Available online 10 July 2023

the different phases of the system established a relation between the equilibrium of liquid and vapor mixture with specifications of temperature components of the PSBSD. It is also found that the efficiency of the PSBSD is 38.135% with a distillate yield of 4.280 l/m^{2}day over 24 h cycle.

1. Introduction

Drinking water scarcity is one of the major problems in developing and under-developing countries [1–3]. This problem motivated researchers to develop advanced desalination technologies to convert saline or brackish water into pure water. The most viable and easy technique for the conversion of saline water into distillate water is the solar-based distillation technique [4–6]. Solar distillation is similar to that of the natural convection, evaporation, and condensation process from ponds, lakes, oceans, and seas [7–9]. In solar distillation, solar energy is utilized for the process of distillation of saline/brackish water either by passive or active methods [10–12]. The passive methods include the process of evaporation by natural means and the active method includes the auxiliary heating of saline/brackish water for evaporation and condensation [13,13,14]. Solar distillation is a familiar well-established distillation technique and many designs of solar stills have been tested, however, evaluation methods for the performance and determination of correlated parameters remain a hard-research issue [15–18].

Wang et al. [19] tested a combined system composed of photovoltaic panels integrated with a cooling system for a concentrator with fresnel reflectors of linear type. The thermodynamical analysis of the obtained results indicated that the developed hybrid system has higher overall and conversion efficiencies. It was also reported that there is a computed optimal temperature of the tube collector that maximizes output power and system efficiency. Yang et al. [20] have constructed a solar organic Rankine cycle system and thermodynamically analyze the system with four organic working fluids. Results of the study showed that the temperature of toluene increased and the system reached a maximum efficiency of 17.9%. Xu et al. [21] designed and fabricated a humidification-dehumidification system with a heat pump and thermodynamically analyzed its performance. The analysis has evaluated the highest gained-out ratio of 12.24 with a distillate output of 18.35 kg/kWh. Parsa et al. [22] tested three solar stills with nanoparticles added into the basin with 0.1 wt% concentration. Three different nanoparticles were used namely, TiO_2, Au, and Ag. The performance of the three stills as well as the conventional solar still was analyzed. It has been found that Ag-incorporated solar still has shown better efficiency of 33.68% and exergy efficiency of 2.34% which are higher than the still with other nanoparticles. Shoeibi et al. [23] used nanofluids to lessen the temperature of the condensation glass cover of thermoelectric solar still. Different types of nanofluids with a concentration of 0.9% of Al_2O_3, CuO, TiO_2, or multiwalled carbon nanotube have given higher productivity than the standalone still. Multiwalled carbon nanotubes showed the highest augmentation in the system performance compared with other nanofluids. Lawrence et al. [24] used nickel oxide nanoparticles in a single-slope wick-type solar distiller and tested it under meteorological conditions of Coimbatore, India to assess the absorptivity of the wick material and the still productivity. It has been found that the nighttime productivity has been increased and total productivity of 5.81 l/m^{2}day was obtained. Saxena et al. [25] made a thorough review of the thermodynamic behavior of solar stills. The review has identified the operational parameters with future prospects and potential techniques for the enhancement of the performance of the stills. Ural et al. [26] tested a solar pump heating system supported air heater and thermodynamically analyzed its performance. The analysis has reduced the electrical consumption by 8.3% for the compressor. Eisavi et al. [27] have carried out a thermodynamic and exergy-economic analysis of a desalination system equipped with solar driven air compressor working with an organic rankine cycle. It was found that 79.9% of the total cost is utilized for the exergy destruction with a factor of 20.1%.

Further, for arid climates, a greenhouse has been constructed to provide fresh water and suitable cooling conditions to plants utilizing solar energy [28]. A parabolic trough solar collector was used as an energy source to operate an organic Rankine cycle. The waste thermal energy from this cycle was used to operate the absorption cooling system. The whole system was thermodynamically analyzed. The obtained results of the thermodynamical analysis indicated that the established system could provide 17.5–27.3 m^3/day of fresh water as well as suitable cooling conditions for accelerating plant growth inside the greenhouse. He et al. [29] carried out a thermodynamic analysis of a steam electrolyzer driven by solar energy to produce hydrogen. The carried-out analysis indicated that direct solar irradiance and solar rays incidence angle are the most effective parameters for the operation of the system rather than the relative humidity. A sincere effort has been done to thermodynamically analyze the performance of a u-shaped basin solar still with two slopes incorporated with ZnO/activated carbon nanoparticles using Gibbs free energy at the temperature components of the system by Sangeetha et al. [30]. It was observed that an efficiency of 38.33% is achieved with an output of 14.921 l/m^2 day. Gibbs free energy analysis has proven the improved thermal conductivity of silver balls in the basin of the solar still. Yu et al. [31] developed a numerical simulation model for the thermodynamic behavior of a solar air evaporating system incorporated with a thermal collector and evaporation unit. It was found that the system had an efficiency of 83.0%. Tully et al. [32] used an internal side wall reflector, hollow circular fin, phase change material, and nanoparticle mixed phase change material in a double slope solar distiller and tested it for both active and passive modes. Thermodynamic analysis along with exergy, energy, exergy-economic, environmental, and sustainability has been done and it was proved that nano-PCM saved 2% of the total cost per unit production of water. Okati et al. [33] designed, established, and tested a direct contact membrane distillation unit. Energy, exergy, economic and environmental analysis has been done and inferred that exergy efficiency improved by 48.34% with 15000 m^2/day desalination unit.

Alsaiari et al. [34] tested a solar distiller that had a titanium oxide/jackfruit peel paint mixture in varying ratios (0.1%, 0.2%, and 0.3%). Steel balls of silver color loaded with hybrid nanofluids were introduced into the solar still basin to improve the heat transmission process. The obtained water yield reached a high value of 8.7919 l/m^{2}day.

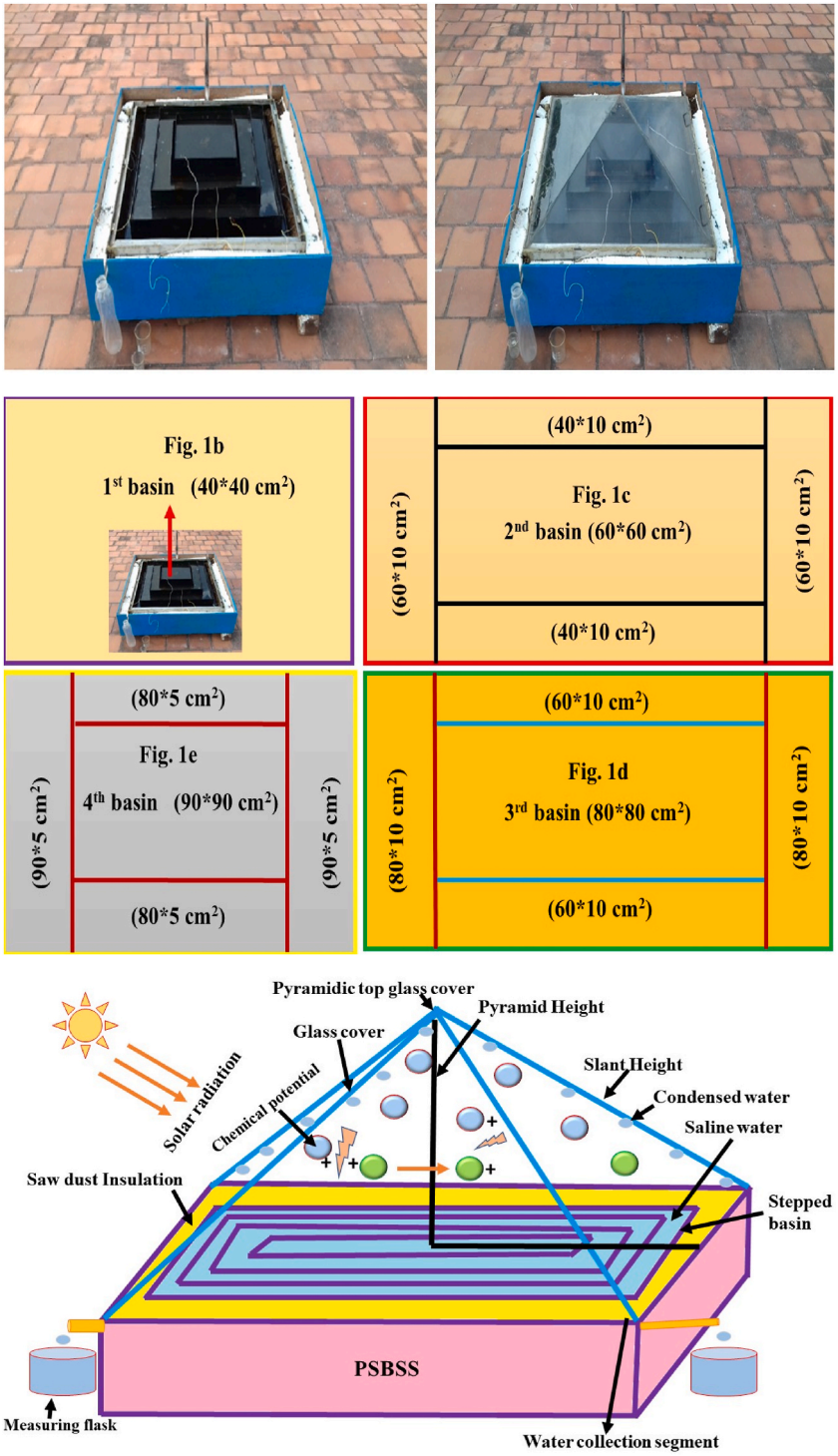

Fig. 1. aPhotograph of the PSBSS.
Fig. 1(b to e): Schematic diagram in 2D view of the PSBSS.
Fig. 1f: Schematic diagram of the PSBSS.

Dhivagar et al. [35] carried out a thermodynamic analysis of both conventional distiller and biomass evaporator-assisted solar distiller containing crushed gravel. The study revealed that the biomass evaporator-assisted solar distiller containing crushed gravel has obtained energy destruction of 12% and 22% for basin and saline water with an entropy of 60.7% higher than conventional solar distiller. Wang et al. [36] carried out experiments on thermal systems composed of thermal and photovoltaic energy and developed a

thermodynamic model to assess the thermal behavior of the system. The analysis has shown the negative role of solar radiation intensity on power production by photovoltaic modules. Prasanna et al. [37] have used various basin materials in the basin of a solar distiller incorporated with an air cavity and undergone exergy, energy, and economic analysis to determine the payback period of the distiller as well as the cost per liter of drinking water. It was found that the payback period was found to be 10 min and Rs. 0.723 per liter. Sharshir et al. [38] constructed a hemispherical solar still with a V-corrugated basin to hold wick material and a thermo-economic analysis of the system was done. The analysis revealed that the total heat transfer coefficient increased by 55% with thermal and exergy efficiency of 39.75% and 44.04%.

The drawbacks of distillers are their small output yield (around 3 l/day) and low efficiency (about 30%). So, various kinds of solar stills were proposed in an attempt to avoid the drawbacks of conventional stills (CSS). As a result, different designs were reported in the literature such as dish solar distillers [39], double-effect stills [40], and triangular solar still [41]. Lawrenece et al. [42] carried out a simulation study to assess the performance of a single slope solar still in four coastal locations in India, namely Chennai, Visakhapatnam, Trivandrum, and Mumbai. Lawrence et al. [24] studied the effect of the introduction of nickel oxide nanoparticles in the single slope wick type solar still and inferred that there is a significant enhancement of absorption of solar radiation for effective evaporation inside the solar still. Shanmugasundaram and Janarthanan [43] have experimented with the honeycomb double-exposure solar still and proposed a model for the thermal asymmetries taking place inside the solar still. Shahin Shoeibi et al. [44] developed a new design of a hybrid solar desalination system integrated with an external condenser by using a wind ventilator and water cooling system after that modification improved CO_2 mitigation 2.03 times. Overall system per day yield of the modified solar still was enhanced by 213%. Followed Shahin Shoeibi et al. [13] have designed and fabricated a new evacuated tube heat pipe solar collector integrated with a solar still incorporated with external condenser for the performance in terms of distillate yield. It has been found that the new still has produced distillate output higher than the conventional solar still.

Ramasamy Dhivagar et al. [13] used black iron oxide magnetic power particles with the water in the basin of the modified solar still. It has been found that the still with magnetic powder has produced a distillate yield that is 31.2% higher than the ordinary conventional solar still.

Analysis of solar still using energy matrices which are incorporated with a cooling fan has been done by Shahin Shoeibi et al. [45]. Results of the study have shown that freshwater production, energy efficiency, and exergy efficiency increased by 79%, 11%, and 45% respectively. Shahin Shoeibi et al. [46] have compared the CFD simulation model for double-slope solar still, hemispherical solar still, and tubular solar still using nanofluid film cooling. The solar desalination with nanofluids film cooling had a higher yield by about 4.8% compared to other solar desalination systems (hemispherical solar still, and tubular solar still). All solar distillers used net CO_2 mitigation of 14.08 tons (double-slope), 13.72 tons (hemispherical), and 13.44 tons (tubular). Further Shoeibi et al. [47] have made a thorough review of the performance evaluation of solar desalination integrated with heat pipes.

In the present work, a pyramid solar still with a stepped basin has been designed, fabricated, and tested. The basin of the PSBSD has been filled with saline water and activated carbon prepared from mango tree wood to increase the absorptivity of water in the basin.

Analytical solutions for the temperature components of the still based on the energy balance equations have been evaluated and change in the internal energy has been attempted. Gibbs free energy equation has been proposed for the determination of the change in energy between the evaporating and condensing phases at a steady state. The chemical potential is evaluated using the Gibbs free energy in the steady state equilibrium and the variation in the chemical potential between the two phases has been tried to identify the thermal behavior of the still. Moreover, the performance of the still has been explained precisely with the values of the chemical potential. Further, the thermographic diagrams of the temperature components of the PSBSD to implement the Gibbs phase rule for the identification of phase change during evaporation and condensation.

2. Solar distiller design

A square pyramid distiller was designed and established with a main body made of low-carbon steel. The basin depth was 0.12 m. The distiller basin was covered with an inclined glass cover with transparency optical characteristics and a thickness of 0.004 m. This cover is composed of four components forming a pyramid shape. The basin had a copper sheet metal which acted as an absorber plate. The copper sheet was coated with black paint and had an absorbing area of 1 m^2. All internal surfaces of the distiller side wall were also coated with black paint to maximize the absorbed solar energy which is consequently converted into thermal energy. The distiller was made of two plywood enclosures. There was a 0.05 m gap between the enclosures. This gap was filled with glass wool which acted as a thermal insulator. This filler lessened the heat dissipated to the environment due to its low thermal conductivity (0.00037 W/mK). The pyramid basin had four trays. The upper tray had an outer area of 40*40 cm^2 with an effective evaporating area of 0.16 m^2. The second tray had an outer area of 60*60 cm^2 with an effective evaporating area of 0.20 m^2. The third tray had an outer area of 80*80 cm^2 with an effective evaporating area of 0.28 m^2. The lower tray had an outer area of 90*90 cm^2 with an effective evaporating area of 0.17 m^2. The saline water was fed into the distiller using a piping system containing control valves with an elevation of 0.05 m from the distiller base. Fig. 1a shows the photograph of the PSBSD.

Four basin trays with unequal evaporation areas were established inside the distiller trough to divide the basin thermal capacity into smaller portions so that the temperature of the water in the basins could be increased as faster as possible. The total thermal capacity of the water in the basin is divided into four basins to fasten the evaporation rate. That is, in each basin, the water heater capacity is small and therefore the radiation is absorbed and rapidly increases the temperature of the water in the basin. It is represented in Fig. 1b–e respectively. 1f shows the schematic representation of the 2D view of the PSBSD. Eight thermocouples were utilized to record the temperature inside the distiller. Four of them were inserted into the saline water of the four trays to record the water in the trays. The others have been attached to the trays to record. The trays' temperature. In addition, four thermocouples were attached

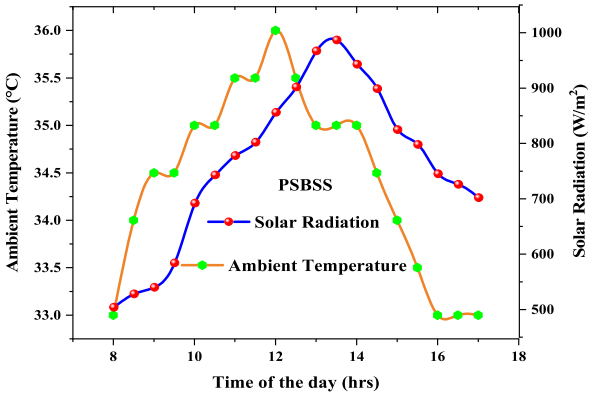

Fig. 2. Change in sunbeam & surrounding air temperatures.

to the outer surfaces of the glass covers to record their temperatures. The distiller trays were filled with 28 L of saline water and divided into four bulks in each tray. The distillate water was collected using four collection channels connected to an external measuring container.

3. Results and discussion

There is a convection, radiation, and evaporative heat transfer from the water in the basins towards the condensation glass cover, water in the four trays absorbs solar energy and the water may be converted into vapors. The solar radiation transmitted through the condensing glass cover reached the water surface of the four basins and the water in the basin absorbs solar radiation followed by the conversion of water into vapors. Since evaporation depends on the intensity of solar radiation, it is considered the influential parameter for evaporation to take place. Moreover, the internal heat transfer of convective, radiative, and evaporative heat transfer occurs inside the solar still and is accompanied by mass transfer. There is a phase change from liquid to gas and again condensed into pure water which is a liquid phase again. This obeys the Gibbs phase rule and it is indispensable to finding the chemical potential. As the first step, the energy balance equations for the temperature components of the PSBSD can be written for the analytical solution.

For PSBSDGlass cover1

$$\propto_g IA_{pg1} + h_1\left(T_{w1} - T_{pg1}\right)A_{w1} = h_{ga}\left(T_{pg1} - T_a\right)A_{pg1} \tag{1}$$

For PSBSD glass cover 2

$$\propto_g IA_{pg2} + h_2\left(T_{w2} - T_{pg2}\right)A_{w2} = h_{ga}\left(T_{pg2} - T_a\right)A_{pg2} \tag{2}$$

For PSBSD glass cover 3

$$\propto_g IA_{pg3} + h_3\left(T_{w3} - T_{pg3}\right)A_{w3} = h_{ga}\left(T_{pg3} - T_a\right)A_{pg3} \tag{3}$$

For PSBSD glass cover 4

$$\propto_g IA_{pg4} + h_4\left(T_{w4} - T_{pg4}\right)A_{w4} = h_{ga}\left(T_{pg4} - T_a\right)A_{pg4} \tag{4}$$

For Evaporating water in basin 1

$$\propto_w IA_{w1} = M_w C_w \frac{dT_{w1}}{dt} + h_1\left(T_{w1} - T_{pg1}\right)A_{w1} + h_b(T_{w1} - T_a)A_{w1} \tag{5}$$

For Evaporating water in basin 2

$$\propto_w IA_{w2} = M_w C_w \frac{dT_{w2}}{dt} + h_2\left(T_{w2} - T_{pg2}\right)A_{w2} + h_b(T_{w2} - T_a)A_{w2} \tag{6}$$

For Evaporating water in basin 3

$$\propto_w IA_{w3} = M_w C_w \frac{dT_{w3}}{dt} + h_3\left(T_{w3} - T_{pg3}\right)A_{w3} + h_b(T_{w3} - T_a)A_{w3} \tag{7}$$

For Evaporating water in basin 4

$$\propto_w IA_{w4} = M_w C_w \frac{dT_{w4}}{dt} + h_4\left(T_{w4} - T_{pg4}\right)A_{w4} + h_b(T_{w4} - T_a)A_{w4} \tag{8}$$

These energy balance equations can be solved for the analytical solution for the water temperature in the four trays and four sides PSBSD glass cover. It has been found that the thermal capacity of the water in the trays has been divided into four trays and four PSBSD

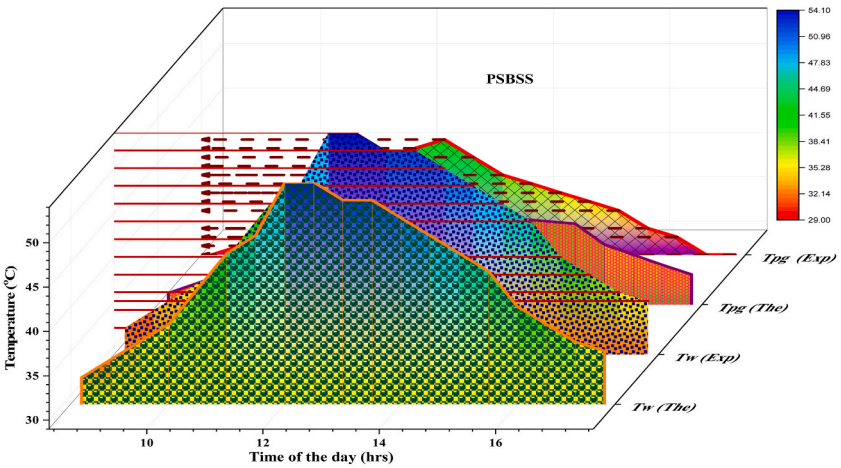

Fig. 3. Investigational standards calculated in water and glass cover temperature together with their cluster for the working hours.

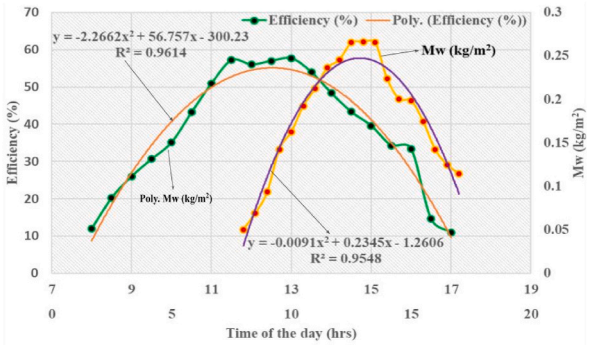

Fig. 4. Shows the immediate distillate yield and efficiency realized for the PSBSS.

glass cover has a similar temperature. Therefore, the average of four PSBSD glass cover temperatures and water temperatures in the basin has been considered and used for the evaluation of distillate yield and efficiency. The significant operational parameter is the intensity of solar radiation which influences the evaporative heat transfer from the evaporating surface to the condensing glass cover surface.

From the analytical solution of the temperature components of the distiller, theoretical values have been evaluated and compared with the obtained experimental observations. Fig. 2 represents the variation of air temperature and solar radiation with respect to time for one of the typical days in May 2022. From the Figure, it is observed that it is a clear sunny day in which the maximum solar radiation of 987 W/m^2 is reached at 13.30 h with an ambient temperature of 36 °C. It is seen that; the intensity of solar radiation gradually increases during morning hours and decreases during evening hours. The intermittent nature of solar radiation is supplying the thermal energy required for the PSBSD to give optimum output. Fig. 3 represents the theoretical and experimental values of the temperature components of the distiller. From the figure, it is observed that there exists a cluster of variation with the correlated temperature such as the average PSBSD glass cover temperature and the average temperature of the basin. The internal heat transfer of convective and radioactive heat transfer is accompanied by the most important evaporative heat transfer which is responsible for the mass transfer from the evaporating surface to the condensing glass cover surface. There is a correlation between the glass covert temperature and the temperature of the trays which in turn is influenced by the intensity of solar radiation. The correlation between the two phases has a conjoint trend due to the equal amount of evaporation and condensation that exist between the phases.

Fig. 4 shows the distillate yield and efficiency obtained for the PSBSD. It is observed that the total distillate yield of 3.380 kg/m^2 during daytime and nighttime output of 0.900 kg/m^2 with a total of 4.280 kg/m^{2}day. The daily average efficiency of 38.13% is obtained for the PSBSDwhich is higher than the conventional pyramid solar distiller. This is due to the fact that the larger thermal capacity of the single basin is divided among the four basins and faster evaporation takes place in all the basins to give maximum output. The polynomial equations have been derived for the amount of distillate water and efficiency which can be utilized for futuristic prediction for any day of the year with minimum error.

The polynomial equations and R^2 values are.

For distillate yield

$$y = -0.0091x^2 + 0.2345x - 1.2606$$

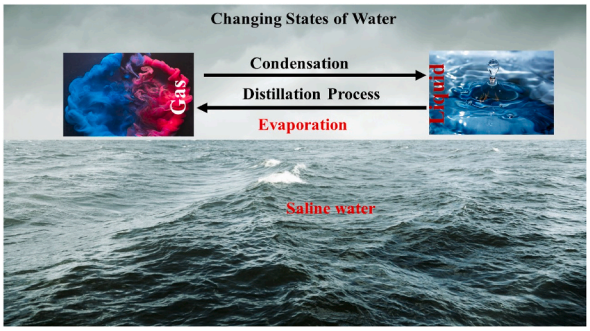

Fig. 5. Variation of different phases while a distillation process takes place in the PSBSS.

$R^2 = 0.9548$

For efficiency

$y = -2.2662x^2 + 56.757x - 300.23$

$R^2 = 0.9614$

The R^2 value for both the distillate yield and efficiency is near to 1 which clearly reflects the best fit of the trend line.

3.1. Thermodynamical analysis

Following, thermodynamical analysis is carried out by considering the phase transition of liquid into vapor and again into a liquid phase which clearly represents the phase change and can implement the Gibbs phase rule. Fig. 5 represents the diffusive phase equilibrium between evaporation and condensation during the distillation process. It is clear that the saline water in the four basins of PSBSD is treated as one system and the four pyramid condensing glass cover is treated as the second system. Since there is a temperature difference between the two systems, there will be a net energy flow between the two systems. If diffusive equilibrium is not obtained, then there will be no net energy flow between the evaporating and condensing glass cover surface. There is a diffusive equilibrium between the two systems, such that Helmholtz free energy is given by

$$H = H_A + H_B \tag{9}$$

If diffusive equilibrium does not exist, then the net energy flow between the evaporating and condensing glass cover surface will not be pronounced and the evaporation rate does not take place inside the solar still and it is found that the total number of particles in the two systems is constant and is given by

$$N = N_A + N_B \tag{10}$$

Where N is the total number of particles in the two systems A and B.

The Helmholtz free energy will become minimum when the rate of evaporation increases and the mass transformation of saline water into pure water by condensation which means the production of pure water is maximum. With this condition, it is possible that

$$\frac{\partial H}{\partial N} = \frac{\partial H_A}{\partial N_A} + \frac{\partial H_B}{\partial N_B} = 0 \tag{11}$$

Eq. (11) is true for the microcanonical ensembles which are U, V and N. U is equal to that of the Helmholtz free energy and therefore it is clear to determine the chemical potential with respect to the ensembles and is written as

$$\mu = \frac{\partial H}{\partial N} \tag{12}$$

Therefore, it is the Helmholtz free energy per unit particle of the system with different phases. It is also possible to determine the chemical potential in terms of Gibbs free energy which is defined as Gibbs free energy per particle of the two phases of the system and is written as

$$\mu = \frac{\partial G}{\partial N} \tag{13}$$

Following the differential for Helmholtz free energy is written

$$dH = -SdT - pdV - \mu dN \tag{14}$$

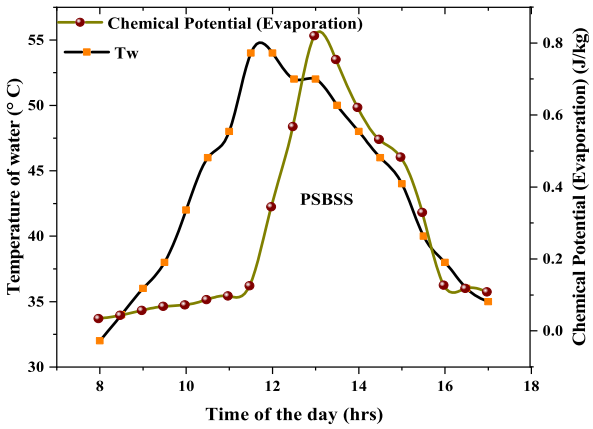

Fig. 6. Chemical potential basin water at its current temperature.

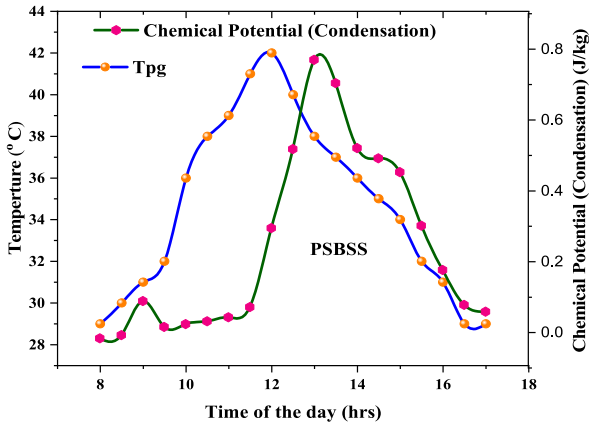

Fig. 7. Shows PSBSS conduction plate chemical potential at temperature.

If μ_A and μ_B are the Gibbs free energy per particle for the two phases, then the diffusive equilibrium between the two phases will be equal and therefor

$$\mu_A = \mu_B \tag{15}$$

Since the particles cannot be divided, the chemical potential can be stated as the finite difference between the Gibbs free energy per particle between the two phases in diffusive contact. Obtaining Gibbs free energy is quite simple and using the free energy, it is possible to find the chemical potential which is the change in free energy of the phases in the system. Therefore, it can be written as

$$\mu = \mu_A - \mu_B \tag{16}$$

Fig. 6 and Fig. 7 represent the chemical potentials at water and glass cover temperatures throughout the working hours of the PSBSD. It has been found the internal energy of the system increases as the chemical potential increases which in turn increases the rate of evaporation. When the internal energy of the evaporating system increases, the phase changes from a liquid into a vapor phase which in turn increases the chemical potential of the condensing glass cover. Moreover, the chemical potential between the two phases can be easily obtained by finding the change in Gibbs free energy between them.

The vapor phase again changes into a liquid phase with the release of latent heat of condensation into the glass cover. It is also seen that the number of particles in the liquid phase is equal to the number of particles in the vapor phase which shows an equilibrium between the two phases. It is due to the fact that the latent heat of vaporization of water vapor is released to the condensing glass cover when it condenses into pure distilled water on the underlying side of the glass condensing glass cover. The difference in chemical potential between the two phases is influenced by the intensity of solar radiation and it is found that the average difference in chemical potential between systems A and B is 0.040 J/kg. The difference in chemical potential between the two phases is small due to the release of latent heat of vaporization of water vapor while condensing into distilled water on the underlying side of the condensing glass cover. The implementation of chemical potential establishes a relation between the different phases of the diffusive equilibrium which are glass cover temperature, water temperature, distillate yield, instantaneous efficiency, and intensity of solar radiation. The steady state occurs when the number of particles in the liquid phase at a particular instant is equal to the number of particles in the

gaseous phase. The temperature components and the climatic parameters are correlated and influence the output of distillate yield and efficiency.

A simulation study of the proposed system is going on and the comparisons will be done in the forthcoming work on the solar energy application device as the attempt is the first time to evaluate the chemical potential. As the chemical potential between the two phases has a conjoint trend, it is clear that the rate of evaporation is proportional to the condensation which clearly reflected from the results that the difference in potential is minimum. The relationship between the influential parameter has been inferred with precise results as the theoretical and experimental results for the temperature components of the solar still have not shown much error. As the difference between the chemical potential of the evaporating and condensing phases is small, the results have confirmed the accuracy of the proposed method. For our future work, we recommend applying the proposed methodology along with machine learning approaches [48–50] to model other desalination systems.

4. Conclusion

Based on the obtained results, the following conclusions could be drawn as follows:

(i) The implementation of chemical potential reflects the significance of the thermodynamic analysis of the PSBSD.
(ii) The average chemical potential difference between the condensing and evaporating surface temperature is found to be 0.040 J/kg.
(iii) The difference in chemical potential between the two phases throughout the working hours of the day with 30-min interval do not exceed 0.060 J/kg which clearly shows the saturation mode of operation of the PSBSD.
(iv) Gibbs phase rule between the diffusive phase establishes the correlation between the two systems.
(v) The daily average efficiency of 38.135% with a yield of 4.280 l/m^{2}day was obtained for the PSBSDwhich is found to be higher than the ordinary basin solar distiller.

Author statement

All authors contributed equally to this work.

Declaration of competing interest

The authors declare that they have no known competing financial interests or personal relationships that could have appeared to influence the work reported in this paper.

Data availability

No data was used for the research described in the article.

Acknowledgement

The authors extend their appreciation to Imam Mohammad Ibn Saud Islamic University, Kingdom of Saudi Arabia, for funding this research work through Grant No. (221414004).

Nomenclature

$\propto_g$	Absorptivity of condensing pyramid glass cover
$\propto_w$	Absorptivity of water in the basin
I	Solar radiation at condensing glass cover surface (W/m^2)
A_{pg1}	Area of the condensing glass cover 1 (m^2)
h_1	Total heat transfer coefficient from water basins to glass cover 1 (W/mK)
T_{w1}	Temperature of water in the basin 1 (K)
T_{pg1}	Temperature of pyramid glass cover 1 (K)
A_{w1}	Area of the basin 1 (m^2)
h_{ga}	Total heat transfer coefficient from glass cover 1 to ambient (W/mK)
T_a	Temperature of the ambient (K)
A_{pg2}	Area of the condensing glass cover 2 (m^2)
h_2	Total heat transfer coefficient from water basins to glass cover 2 (W/mK)
T_{w2}	Temperature of water in the basin 2 (K)
T_{pg2}	Temperature of pyramid glass cover 2 (K)
A_{w2}	Area of the basin 2 (m^2)
A_{pg3}	Area of the condensing glass cover 3 (m^2)
h_3	Total heat transfer coefficient from water basins to glass cover 3 (W/mK)
T_{w3}	Temperature of water in the basin 3 (K)

T_{pg3} Temperature of pyramid glass cover 3 (K)
A_{w3} Area of the basin 3 (m^2)
A_{pg4} Area of the condensing glass cover 4 (m^2)
h_4 Total heat transfer coefficient from water basins to glass cover 4 (W/mK)
T_{w4} Temperature of water in the basin 4 (K)
T_{pg4} Temperature of pyramid glass cover 4 (K)
A_{w4} Area of the basin 4 (m^2)
M_w Mass of water in four basins (kg)
C_w Specific heat capacity of water (J/kgK)
h_b Total heat transfer coefficient from base of the basin to ambient (W/mK)

References

[1] A.H. Elsheikh, S. Shanmugan, R. Sathyamurthy, A. Kumar Thakur, M. Issa, H. Panchal, T. Muthuramalingam, R. Kumar, M. Sharifpur, Low-cost bilayered structure for improving the performance of solar stills: performance/cost analysis and water yield prediction using machine learning, Sustain. Energy Technol. Assessments 49 (2022), 101783, https://doi.org/10.1016/j.seta.2021.101783.
[2] X. Zhang, P. Ye, Y. Wu, Enhanced technology for sewage sludge advanced dewatering from an engineering practice perspective: a review, J. Environ. Manag. 321 (2022), 115938, https://doi.org/10.1016/j.jenvman.2022.115938.
[3] X. Zhang, C. Shu, M. Fujii, Y. Wu, D. Sun, P. Ye, Y. Bao, Numerical and experimental study on water-heat-salt transport patterns in shallow bare soil with varying salt contents under evaporative conditions: a comparative investigation, J. Hydrol. 621 (2023), 129564, https://doi.org/10.1016/j.jhydrol.2023.129564.
[4] A.H. Elsheikh, H. Panchal, M. Ahmadein, A.O. Mosleh, K.K. Sadasivuni, N.A. Alsaleh, Productivity forecasting of solar distiller integrated with evacuated tubes and external condenser using artificial intelligence model and moth-flame optimizer, Case Stud. Therm. Eng. 28 (2021), 101671, https://doi.org/10.1016/j.csite.2021.101671.
[5] A.H. Elsheikh, V.P. Katekar, O.L. Muskens, S.S. Deshmukh, M.A. Elaziz, S.M. Dabour, Utilization of LSTM neural network for water production forecasting of a stepped solar still with a corrugated absorber plate, Process Saf. Environ. Protect. (2021) 148, https://doi.org/10.1016/j.psep.2020.09.068.
[6] E. Banoqitah, R. Sathyamurthy, E.B. Moustafa, M. Fujii, P. Sudalaimuthu, F. Djouider, H. Elsheikh, A, Enhancement and prediction of a stepped solar still productivity integrated with paraffin wax enriched with nano-additives, Case Stud. Therm. Eng. 49 (2023), 103215, https://doi.org/10.1016/j.csite.2023.103215.
[7] E. Ghandourah, Y.S. Prasanna, A.H. Elsheikh, E.B. Moustafa, M. Fujii, S.S. Deshmukh, Performance prediction of aluminum and polycarbonate solar stills with air cavity using an optimized neural network model by golden jackal optimizer, Case Stud. Therm. Eng. 47 (2023), 103055, https://doi.org/10.1016/j.csite.2023.103055.
[8] H. Abulkhair, S.W. Sharshir, E.B. Moustafa, A. Alsaiari, I.A. Moujdin, A.H. Elsheikh, Thermal performance enhancement of a modified pyramid distiller using different modifications with low-cost materials, Sustain. Energy Technol. Assessments 57 (2023), 103191, https://doi.org/10.1016/j.seta.2023.103191.
[9] A.H. Elsheikh, E.M.S. El-Said, M. Abd Elaziz, M. Fujii, H.R. El-Tahan, Water distillation tower: experimental investigation, economic assessment, and performance prediction using optimized machine-learning model, J. Clean. Prod. 388 (2023), 135896, https://doi.org/10.1016/j.jclepro.2023.135896.
[10] M.E. Zayed, A. Kamal, M.R. Diab, F.A. Essa, O.L. Muskens, M. Fujii, A.H. Elsheikh, Novel design of double slope solar distiller with prismatic absorber basin, linen wicks, and dual parallel spraying nozzles: experimental investigation and energic–exergic-economic analyses, Water (2023) 15.
[11] A.O. Alsaiari, E.B. Moustafa, H. Alhumade, H. Abulkhair, A. Elsheikh, A coupled artificial neural network with artificial rabbits optimizer for predicting water productivity of different designs of solar stills, Adv. Eng. Software 175 (2023), 103315, https://doi.org/10.1016/j.advengsoft.2022.103315.
[12] D. Mevada, H. Panchal, M. Ahmadein, M.E. Zayed, N.A. Alsaleh, J. Djuansjah, E.B. Moustafa, A.H. Elsheikh, K.K. Sadasivuni, Investigation and performance analysis of solar still with energy storage materials: an energy- exergy efficiency analysis, Case Stud. Therm. Eng. 29 (2022), 101687, https://doi.org/10.1016/j.csite.2021.101687.
[13] R. Dhivagar, S. Shoeibi, H. Kargarsharifabad, M.H. Ahmadi, M. Sharifpur, Performance enhancement of a solar still using magnetic powder as an energy storage medium-exergy and environmental analysis, Energy Sci. Eng. 10 (2022) 3154–3166, https://doi.org/10.1002/ese3.1210.
[14] R. Dhivagar, S. Shoeibi, S.M. Parsa, S. Hoseinzadeh, H. Kargarsharifabad, M. Khiadani, Performance evaluation of solar still using energy storage biomaterial with porous surface: an experimental study and environmental analysis, Renew. Energy 206 (2023) 879–889, https://doi.org/10.1016/j.renene.2023.02.097.
[15] E. Ghandourah, H. Panchal, O. Fallatah, H.M. Ahmed, E.B. Moustafa, A.H. Elsheikh, Performance enhancement and economic analysis of pyramid solar still with corrugated absorber plate and conventional solar still: a case study, Case Stud. Therm. Eng. 35 (2022), 101966, https://doi.org/10.1016/j.csite.2022.101966.
[16] A. Bamasag, F.A. Essa, Z.M. Omara, E. Bahgat, A.O. Alsaiari, H. Abulkhair, R.A. Alsulami, A.H. Elsheikh, Machine learning-based prediction and augmentation of dish solar distiller performance using an innovative convex stepped absorber and phase change material with nanoadditives, Process Saf. Environ. Protect. 162 (2022) 112–123, https://doi.org/10.1016/j.psep.2022.03.052.
[17] E.B. Moustafa, A.H. Hammad, A.H. Elsheikh, A new optimized artificial neural network model to predict thermal efficiency and water yield of tubular solar still, Case Stud. Therm. Eng. 30 (2022), 101750, https://doi.org/10.1016/j.csite.2021.101750.
[18] S. Shoeibi, M. Saemian, H. Kargarsharifabad, S. Hosseinzade, N. Rahbar, M. Khiadani, M.M. Rashidi, A review on evaporation improvement of solar still desalination using porous material, Int. Commun. Heat Mass Tran. 138 (2022), 106387, https://doi.org/10.1016/j.icheatmasstransfer.2022.106387.
[19] G. Wang, F. Wang, F. Shen, Z. Chen, P. Hu, Novel design and thermodynamic analysis of a solar concentration PV and thermal combined system based on compact linear fresnel reflector, Energy 180 (2019) 133–148, https://doi.org/10.1016/j.energy.2019.05.082.
[20] J. Yang, J. Li, Z. Yang, Y. Duan, Thermodynamic analysis and optimization of a solar organic rankine cycle operating with stable output, Energy Convers. Manag. 187 (2019) 459–471, https://doi.org/10.1016/j.enconman.2019.03.021.
[21] H. Xu, X.Y. Sun, Y.J. Dai, Thermodynamic study on an enhanced humidification-dehumidification solar desalination system with weakly compressed air and internal heat recovery, Energy Convers. Manag. 181 (2019) 68–79, https://doi.org/10.1016/j.enconman.2018.11.073.
[22] S.M. Parsa, A. Yazdani, H. Dhahad, W.H. Alawee, S. Hesabi, F. Norozpour, D. Javadi Y, H.M. Ali, M. Afrand, Effect of Ag, Au, TiO2 metallic/metal oxide nanoparticles in double-slope solar stills via thermodynamic and environmental analysis, J. Clean. Prod. 311 (2021), 127689, https://doi.org/10.1016/j.jclepro.2021.127689.
[23] S. Shoeibi, N. Rahbar, A. Abedini Esfahlani, H. Kargarsharifabad, Improving the thermoelectric solar still performance by using nanofluids– experimental study, thermodynamic modeling and energy matrices analysis, Sustain. Energy Technol. Assessments 47 (2021), 101339, https://doi.org/10.1016/j.seta.2021.101339.
[24] A. Lawrence, C. Hariharan, A. Nagamani Prabu, B. Janarthanan, Influence of nickel oxide nanoparticles on the absorption enhancement of solar radiation for effective distillation by single slope wick-type solar still, Mater. Today Proc. 45 (2021) 2357–2363, https://doi.org/10.1016/j.matpr.2020.10.704.
[25] A. Saxena, E. Cuce, A.E. Kabeel, M. Abdelgaied, V. Goel, A thermodynamic review on solar stills, Sol. Energy 237 (2022) 377–413, https://doi.org/10.1016/j.solener.2022.04.001.
[26] T. Ural, A. Keçebaş, O.V. Güler, Thermodynamic performance evaluation of a heat pump system with textile based solar air heater for heating process, Appl. Therm. Eng. 191 (2021), 116905, https://doi.org/10.1016/j.applthermaleng.2021.116905.

[27] B. Eisavi, H. Nami, M. Yari, F. Ranjbar, Solar-driven mechanical vapor compression desalination equipped with organic rankine cycle to supply domestic distilled water and power – thermodynamic and exergoeconomic implications, Appl. Therm. Eng. 193 (2021), 116997, https://doi.org/10.1016/j.applthermaleng.2021.116997.
[28] F. Mahmood, T.A. Al-Ansari, Design and thermodynamic analysis of a solar powered greenhouse for arid climates, Desalination 497 (2021), 114769, https://doi.org/10.1016/j.desal.2020.114769.
[29] W. He, M.M. Namar, Z. Li, A. Maleki, I. Tlili, M. Safdari Shadloo, Thermodynamic analysis of a solar-driven high-temperature steam electrolyzer for clean hydrogen production, Appl. Therm. Eng. 172 (2020), 115152, https://doi.org/10.1016/j.applthermaleng.2020.115152.
[30] A. Sangeetha, S. Shanmugan, S. Gorjian, Experimental evaluation and thermodynamic Gibbs free energy analysis of a double-slope U-shaped stepped basin solar still using activated carbon with ZnO nanoparticles, J. Clean. Prod. 380 (2022), 135118, https://doi.org/10.1016/j.jclepro.2022.135118.
[31] J. Yu, J. Yang, W. Yan, Thermodynamic simulation and experiment research of the solar air evaporating separation system for saline wastewater treatment with thermal collector–evaporator integrated unit, Energy Rep. 8 (2022) 6707–6728, https://doi.org/10.1016/j.egyr.2022.05.025.
[32] S.S. Tuly, M.S. Islam, R. Hassan, B.K. Das, M.R.I. Sarker, Investigation of a modified double slope solar still integrated with nanoparticle-mixed phase change materials: energy, exergy, exergo-economic, environmental, and sustainability analyses, Case Stud. Therm. Eng. 37 (2022), 102256, https://doi.org/10.1016/j.csite.2022.102256.
[33] V. Okati, A.J. Moghadam, M. Farzaneh-Gord, M. Moein-Jahromi, Thermo-economical and environmental analyses of a direct contact membrane distillation (DCMD) performance, J. Clean. Prod. 340 (2022), 130613, https://doi.org/10.1016/j.jclepro.2022.130613.
[34] A.O. Alsaiari, S. Shanmugan, H. Abulkhair, A. Bamasag, E.B. Moustafa, R.A. Alsulami, I. Ahmad, A. Elsheikh, Applications of TiO2/jackfruit peel nanocomposites in solar still: experimental analysis and performance evaluation, Case Stud. Therm. Eng. 38 (2022), 102292, https://doi.org/10.1016/j.csite.2022.102292.
[35] R. Dhivagar, B. Deepanraj, M. Mohanraj, H. Chyuan Ong, Second law based thermodynamic analysis of crushed gravel sand and biomass evaporator assisted solar still, Sustain. Energy Technol. Assessments 52 (2022), 102160, https://doi.org/10.1016/j.seta.2022.102160.
[36] J. Wang, H. Chen, H. Deng, F. Dong, A combined power and steam system integrated with solar photovoltaic/thermal collector: thermodynamic characteristics and cost-benefit analyses, Case Stud. Therm. Eng. 39 (2022), 102477, https://doi.org/10.1016/j.csite.2022.102477.
[37] Y.S. Prasanna, S.S. Deshmukh, Energy, exergy and economic analysis of an air cavity appended passive solar still of different basin material at varying depth, Energy Sustain. Dev. 71 (2022) 13–26, https://doi.org/10.1016/j.esd.2022.09.008.
[38] S.W. Sharshir, M.A. Omara, G. Elsisi, A. Joseph, A.W. Kandeal, A. Ali, G. Bedair, Thermo-economic performance improvement of hemispherical solar still using wick material with V-corrugated basin and two different energy storage materials, Sol. Energy 249 (2023) 336–352, https://doi.org/10.1016/j.solener.2022.11.038.
[39] B.F. Felemban, F.A. Essa, A. Afzal, M.H. Ahmed, B. Saleh, H. Panchal, S. Shanmugan, A. Elsheikh, Z.M. Omara, Experimental investigation on dish solar distiller with modified absorber and phase change material under various operating conditions, Environ. Sci. Pollut. Res. 29 (2022) 63248–63259, https://doi.org/10.1007/s11356-022-20285-z.
[40] R. Kumar, J. Chanda, H. Elsheikh, A, B. Ongar, Y. Khidolda, S. PraveenKumar, H. Panchal, S. Shanmugan, Performance improvement of single and double effect solar stills with silver balls/nanofluids for bioactivation: an experimental analysis, Sol. Energy 259 (2023) 452–463, https://doi.org/10.1016/j.solener.2023.05.012.
[41] N.Y.Y. Emran, A. Ahsan, E.H.H. Al-Qadami, M.M. El-Sergany, M. Shafiquzzaman, M. Imteaz, A.W.M. Ng, M.A.U.R. Tariq, S. Idrus, Z. Mustaffa, et al., Efficiency of a triangular solar still integrated with external PVC pipe solar heater and internal separated condenser, Sustain. Energy Technol. Assessments 52 (2022), 102258, https://doi.org/10.1016/j.seta.2022.102258.
[42] A. Lawrence, C. Hariharan, S. Shanmugan, B. Janarthanan, Performance of single slope solar still for socio-economic development in coast locations in India, Int. J. Ambient Energy 43 (2022) 5175–5183, https://doi.org/10.1080/01430750.2021.1927838.
[43] K. Shanmugasundaram, B. Janarthanan, Modeling thermal asymmetries in honeycomb double exposure solar still, in: Proceedings of the Emerging Trends in Science, Engineering and Technology: Proceedings of International Conference, INCOSET 2012, Springer, 2012, pp. 579–593.
[44] S. Shoeibi, H. Kargarsharifabad, N. Rahbar, G. Khosravi, M. Sharifpur, An integrated solar desalination with evacuated tube heat pipe solar collector and new wind ventilator external condenser, Sustain. Energy Technol. Assessments 50 (2022), 101857.
[45] S. Shoeibi, N. Rahbar, A. Abedini Esfahlani, H. Kargarsharifabad, Energy matrices, economic and environmental analysis of thermoelectric solar desalination using cooling fan, J. Therm. Anal. Calorim. 147 (2022) 9645–9660, https://doi.org/10.1007/s10973-022-11217-7.
[46] S. Shoeibi, S. Ali Agha Mirjalily, H. Kargarsharifabad, H. Panchal, R. Dhivagar, Comparative study of double-slope solar still, hemispherical solar still, and tubular solar still using Al2O3/water film cooling: a numerical study and CO2 mitigation analysis, Environ. Sci. Pollut. Res. 29 (2022) 65353–65369.
[47] S. Shoeibi, S.A.A. Mirjalily, H. Kargarsharifabad, M. Khiadani, H. Panchal, A comprehensive review on performance improvement of solar desalination with applications of heat pipes, Desalination 540 (2022), 115983, https://doi.org/10.1016/j.desal.2022.115983.
[48] E.B. Moustafa, A. Elsheikh, Predicting characteristics of dissimilar laser welded polymeric joints using a multi-layer perceptrons model coupled with archimedes optimizer, Polymers (2023) 15.
[49] A. Elsheikh, Bistable morphing composites for energy-harvesting applications, Polymja (2022) 14.
[50] A.H. Elsheikh, Applications of machine learning in friction stir welding: prediction of joint properties, real-time control and tool failure diagnosis, Eng. Appl. Artif. Intell. 121 (2023), 105961, https://doi.org/10.1016/j.engappai.2023.105961.